Journal of the Mechanics and Physics of Solids 66 (2014) 42–58

Contents lists available at ScienceDirect

Journal of the Mechanics and Physics of Solids

journal homepage: www.elsevier.com/locate/jmps

Thermomechanics of monolayer graphene: Rippling, thermal expansion and elasticity

Wei Gao, Rui Huang*

Department of Aerospace Engineering and Engineering mechanics, University of Texas, Austin, TX 78712, USA

ARTICLE INFO

Article history:
Received 15 September 2013
Received in revised form
1 December 2013
Accepted 28 January 2014
Available online 15 February 2014

Keywords:
Graphene
Thermal expansion
Elasticity
Molecular dynamics
Statistical mechanics

ABSTRACT

Thermomechanical properties of monolayer graphene with thermal fluctuation are studied by both statistical mechanics analysis and molecular dynamics (MD) simulations. While the statistical mechanics analysis in the present study is limited by a harmonic approximation, significant anharmonic effects are revealed by MD simulations. The amplitude of out-of-plane thermal fluctuation is calculated for graphene membranes under both zero stress and zero strain conditions. It is found that the fluctuation amplitude follows a power-law scaling with respect to the linear dimension of the membrane, but the roughness exponents are different for the two conditions due to anharmonic interactions between bending and stretching modes. Such thermal fluctuation or rippling is found to be responsible for the effectively negative in-plane thermal expansion of graphene at relatively low temperatures, while a transition to positive thermal expansion is predicted as the anharmonic interactions suppress the rippling effect at high temperatures. Subject to equi-biaxial tension, the amplitude of thermal rippling decreases nonlinearly, and the in-plane stress-strain relation of graphene becomes nonlinear even at infinitesimal strain, in contrast with classical theory of linear elasticity. It is found that the tangent biaxial modulus of graphene depends on strain non-monotonically, decreases with increasing temperature, and depends on membrane size. Both statistical mechanics and MD simulations suggest considerable entropic contribution to the thermomechanical properties of graphene, and as a result thermal rippling is intricately coupled with thermal expansion and thermoelasticity for monolayer graphene membranes.

1. Introduction

As a two-dimensional crystal membrane, graphene has drawn tremendous interests for research and applications. Among its many unique properties, the mechanical properties of graphene combine high in-plane stiffness and high strength (Lee et al., 2008) with extremely low flexural stiffness (Lu et al., 2009), rendering a highly deformable but robust membrane material. Experimental observations have found that suspended graphene membranes often display spontaneous ripples (Meyer et al., 2007; Bangert et al., 2009; Zan et al., 2012). Theoretically, different physical origins for rippling have been proposed. Thompson-Flagg et al. (2009) suggested that the rippling could be a consequence of adsorbed OH molecules on random sites. On the other hand, thermal fluctuation has been considered as a reasonable explanation for intrinsic ripples in graphene (Fasolino et al., 2007;

* Corresponding author.
E-mail address: ruihuang@mail.utexas.edu (R. Huang).

http://dx.doi.org/10.1016/j.jmps.2014.01.011
0022-5096

Abedpour et al., 2007). In the present study, we focus on the effects of thermal fluctuation on thermomechanical properties of monolayer graphene, including thermal expansion and temperature-dependent elastic modulus.

The basic mechanical properties of graphene have been reasonably understood, including elastic moduli for in-plane extension and bending. However, the effect of temperature on the mechanical properties of graphene is not well understood. The fact that the elastic moduli measured at the room temperature ($T\sim 300$ K) are in close agreement with theoretical values predicted at $T=0$ K may imply insignificant temperature dependence for the elastic moduli. By molecular dynamics (MD) simulations, Zhao and Aluru (2010) predicted that Young's modulus of graphene does not vary significantly with temperature up to about 1200 K, beyond which graphene becomes more compliant. On the other hand, by means of atomistic Monte Carlo (MC) simulations, Zakharchenko et al. (2009) predicted a non-monotonic behavior of shear modulus of graphene with a maximum at about 900 K, and Chen and Chrzan (2011) predicted monotonic decrease of the elastic modulus of graphene with temperature up to 4000 K. Since graphene spontaneously fluctuates out-of-plane at a finite temperature, the effective in-plane elastic modulus is expected to depend on the significance of thermal fluctuation. Another manifestation of out-of-plane thermal fluctuation is possible reduction of the projected area, which has been suggested as the cause for negative in-plane thermal expansion of graphene (Zakharchenko et al., 2009; Chen and Chrzan, 2011). Based on density-functional-theory (DFT) calculations and a quasiharmonic approximation (QHA), Mounet and Marzari (2005) predicted negative in-plane thermal expansion for graphite and graphene, which was attributed to the lowest transversal acoustic (ZA) phonon modes (also called bending modes). Negative thermal expansion of graphene was also predicted by a nonequilibrium Green's function approach (Jiang et al., 2009) and *ab initio* molecular dynamics (AIMD) simulations (Pozzo et al., 2011). Experimentally, Bao et al. (2009) measured thermal expansion of suspended graphene by SEM imaging between 300 and 400 K, with a transition from negative to positive coefficient of thermal expansion (CTE). Based on frequency measurements of suspended graphene electromechanical resonators, Singh et al. (2010) extracted negative CTEs for graphene between 300 and 30 K. Considerable discrepancies remain between the experimental measurements and theoretical predictions for CTE of graphene.

The present work combines MD simulations of graphene with a statistical mechanics (SM) approach for the study of thermomechanical properties of monolayer graphene. The SM approach has been used extensively for the study of flexible membranes (Bowick and Travesset, 2001; Nelson et al., 2004; Freund, 2013), primarily for biological membranes. With relatively simple atomistic structures in graphene, it is possible to directly sample the statistical behavior of graphene membranes with atomistic details to compare with theoretical SM analysis (Los et al., 2009; Zakharchenko et al., 2010), hence opening a new paradigm for the study of membrane physics. The rest of this paper is organized as follows. A theoretical approach based on statistical mechanics of a continuum elastic membrane is presented in Section 2. Section 3 describes the MD simulation method. In Section 4, the results from MD simulations are discussed in comparison with the theoretical analysis. Section 5 summarizes the results and findings.

2. Statistical mechanics of graphene

2.1. A continuum membrane model

Consider monolayer graphene as a continuum membrane with a two-dimensional (2D) reference configuration in the ground state at $T=0$ K. The in-plane dimensions of the graphene membrane are much larger than the atomic length scales (e.g., the bond length, $r_0\sim 0.142$ nm), while the monatomic thickness is undefined (and unnecessary) in the continuum model. The kinematics of general thermomechanical deformation can be described by an in-plane Green–Lagrange strain tensor and a curvature tensor, based on a 2D to 3D mapping (Arroyo and Belytschko, 2002; Lu and Huang, 2009). Under the assumption of relatively small deformation but with moderately large out-of-plane deflection, the in-plane strain and curvature are approximately

$$\varepsilon_{\alpha\beta}=\frac{1}{2}\left(\frac{\partial u_\alpha}{\partial x_\beta}+\frac{\partial u_\beta}{\partial x_\alpha}+\frac{\partial w}{\partial x_\alpha}\frac{\partial w}{\partial x_\beta}\right), \tag{1}$$

and

$$\kappa_{\alpha\beta}=\frac{\partial^2 w}{\partial x_\alpha \partial x_\beta}, \tag{2}$$

where the Greek subscript (α or β) represents x or y for the in-plane coordinates, u_x and u_y are in-plane displacements, and w is out-of-plane deflection. It is noted that the strain tensor in Eq. (1) includes a nonlinear contribution from the out-of-plane deflection that leads to geometric coupling between the in-plane and out-of-plane deformation modes. The kinematics is identical to the von Karman nonlinear plate theory (Timoshenko and Woinowsky-Krieger, 1987).

The total potential energy of the membrane consists of two parts: in-plane strain energy and bending energy. Under the condition of small deformation, the strain energy density function can be written as

$$\Phi(\boldsymbol{\varepsilon},\boldsymbol{\kappa})=\Phi_\varepsilon(\boldsymbol{\varepsilon})+\Phi_\kappa(\boldsymbol{\kappa}), \tag{3}$$

where

$$\Phi_\varepsilon = \frac{E}{2(1+\nu)}\left(\varepsilon_{\alpha\beta}\varepsilon_{\alpha\beta} + \frac{\nu}{1-\nu}\varepsilon_{\alpha\alpha}\varepsilon_{\beta\beta}\right), \tag{4}$$

$$\Phi_\kappa = \frac{1}{2}DI_\kappa^2 - D_G II_\kappa = \frac{D-D_G}{2}\kappa_{\alpha\alpha}\kappa_{\beta\beta} + \frac{D_G}{2}\kappa_{\alpha\beta}\kappa_{\alpha\beta}. \tag{5}$$

Four elastic constants are used in the above equations, including the 2D Young's modulus E (unit: N/m), Poisson's ratio ν, bending modulus D, and Gaussian curvature modulus D_G. They are all defined for the potential energy in the ground state, thus independent of temperature. Note that the bending strain energy density Φ_κ is written as a function of the two invariants of the curvature tensor (Helfrich, 1973): $I_\kappa = \kappa_{11} + \kappa_{22}$ and $II_\kappa = \kappa_{11}\kappa_{22} - \kappa_{12}^2$; the first invariant is twice of the mean curvature, and the second invariant is Gaussian curvature. In classical plate theory (Timoshenko and Woinowsky-Krieger, 1987), both bending moduli (D and D_G) can be related to the in-plane Young's modulus and Poisson's ratio. For graphene, however, they are determined from atomistic modeling as independent constants (Koskinen and Kit, 2010; Wei et al., 2012). As discussed in a previous study (Lu et al., 2009), the physical origin of the bending moduli of monolayer graphene is fundamentally different from that in classical plate theory.

As noted by Helfrich (1973) in the study of lipid bilayers, the bending energy due to Gaussian curvature depends solely on boundary conditions and can be ignored in most cases. Therefore, the total bending energy of a membrane can be written as an area integral:

$$U_b = \iint_\Omega \Phi_\kappa dxdy = \frac{D}{2}\iint_\Omega \left(\frac{\partial^2 w}{\partial x^2} + \frac{\partial^2 w}{\partial y^2}\right)^2 dxdy \tag{6}$$

where Ω is the area of the membrane in the reference state. In the present work, we extend the Helfrich membrane model to study thermomechanical properties of graphene, in comparison with MD simulations.

The mechanical properties of graphene in the ground state ($T=0$ K) have been predicted by DFT calculations (Kudin et al., 2001): $E=345$ N/m, $\nu=0.15$, and $D=1.5$ eV. However, the empirical potential used in the MD simulations yields different values (Lu and Huang, 2009): $E=243$ N/m, $\nu=0.397$, and $D=1.4$ eV. The second set of mechanical properties is used when comparing the theoretical predictions with MD simulations. Despite the discrepancy in the 2D Young's modulus, the predictions for the 2D biaxial modulus, $E^* = E/(1-\nu)$, are in close agreement between the empirical potential ($E^* \sim 403$ N/m) and DFT ($E^* \sim 406$ N/m).

2.2. Out-of-plane thermal fluctuation

Now consider a square-shaped graphene membrane of side length L_0 in the ground state. At a finite temperature but subject to no external force, the membrane fluctuates with both in-plane and out-of-plane modes. In this section we consider out-of-plane thermal fluctuation only. Assuming periodic boundary conditions, the lateral deflection can be written in form of the Fourier series:

$$w(\mathbf{r}) = \sum_k \hat{w}(\mathbf{q}_k) e^{i\mathbf{q}_k \cdot \mathbf{r}}, \tag{7}$$

and the Fourier coefficients are

$$\hat{w}(\mathbf{q}_k) = \frac{1}{L_0^2}\iint_\Omega w(\mathbf{r}) e^{-i\mathbf{q}_k \cdot \mathbf{r}} d\Omega, \tag{8}$$

where $\mathbf{r}$ is the 2D position vector in the ground state and $\mathbf{q}_k$ denotes the k-th wave vector in the 2D space.

Substituting Eqs. (7) into (6) and applying the Parseval theorem (Kammler, 2007), we obtain the bending energy of the membrane in terms of the Fourier coefficients

$$U_b = \frac{DL_0^2}{2}\sum_k q_k^4 [\hat{w}_{\mathrm{Re}}^2(\mathbf{q}_k) + \hat{w}_{\mathrm{Im}}^2(\mathbf{q}_k)], \tag{9}$$

where $q_k = |\mathbf{q}_k|$, $\hat{w}_{\mathrm{Re}}(\mathbf{q}_k)$ and $\hat{w}_{\mathrm{Im}}(\mathbf{q}_k)$ are the real and imaginary parts of $\hat{w}(\mathbf{q}_k)$, respectively.

For a statistical treatment, $\hat{w}_{\mathrm{Re}}(\mathbf{q}_k)$ and $\hat{w}_{\mathrm{Im}}(\mathbf{q}_k)$ are taken as continuous random variables. Each set of $\hat{w}_{\mathrm{Re}}(\mathbf{q}_k)$ and $\hat{w}_{\mathrm{Im}}(\mathbf{q}_k)$ constitutes a possible configuration of the membrane. All possible configurations of the membrane construct a statistical ensemble. It is important to note that the Fourier coefficients $\hat{w}(\mathbf{q}_k)$ and $\hat{w}(-\mathbf{q}_k)$ are not independent. Since $w(\mathbf{r})$ is real-valued in Eq. (8), it can be shown that

$$\hat{w}_{\mathrm{Re}}(\mathbf{q}_k) = \hat{w}_{\mathrm{Re}}(-\mathbf{q}_k) \ \text{ and } \ \hat{w}_{\mathrm{Im}}(\mathbf{q}_k) = -\hat{w}_{\mathrm{Im}}(-\mathbf{q}_k). \tag{10}$$

Consequently, only those Fourier coefficients associated with the upper half-plane of the wave vectors (i.e., $\mathbf{q}_k \cdot \mathbf{e}_y \geq 0$, including only half of the x-axis) are taken as independent random variables. It then follows that the bending energy in

Eq. (9) can be written in terms of the independent random variables as

$$U_b = DL_0^2 \sum_{k(\mathbf{q}_k \cdot \mathbf{e}_y \geq 0)} q_k^4 \left[\hat{w}_{\mathrm{Re}}^2(\mathbf{q}_k) + \hat{w}_{\mathrm{Im}}^2(\mathbf{q}_k) \right], \tag{11}$$

where $\mathbf{e}_y$ is the unit vector in the positive direction of y-coordinate.

For each possible configuration, the total potential energy is

$$U = \iint_{\Omega} \Phi(\boldsymbol{\varepsilon}, \boldsymbol{\kappa}) d\Omega = U_b + U_s \tag{12}$$

where $U_s = \iint_{\Omega} \Phi_\epsilon(\varepsilon) d\Omega$. Under the assumption of small deflection, the nonlinear contribution to the in-plane strain in Eq. (1) is neglected. Consequently, the in-plane strain energy U_s is independent of the out-of-plane fluctuation, and the in-plane and out-of-plane modes are decoupled. This is commonly taken as a harmonic approximation.

Based on classical statistical mechanics (Pathria, 1996; Weiner, 2002), the probability density function (PDF) for each configuration is given by Boltzmann distribution at thermal equilibrium:

$$\rho = \frac{1}{Z} \exp\left(-\frac{U}{k_B T} \right), \tag{13}$$

where k_B is the Boltzmann constant, T is the temperature, and Z is the configurational partition function. The partition function is calculated by an integral with respect to all independent random variables (including both the in-plane and out-of-plane modes) for all possible configurations. Under the harmonic approximation, the partition function is simply a product of two parts, namely

$$Z = Z_b Z_s, \tag{14}$$

where the contribution due to the out-of-plane modes is

$$\begin{aligned} Z_b &= \int_{-\infty}^{\infty} \cdots \int_{-\infty}^{\infty} \exp\left(-\frac{U_b}{k_B T} \right) d\hat{w}_{\mathrm{Re}}(\mathbf{q}_1) d\hat{w}_{\mathrm{Im}}(\mathbf{q}_1) d\hat{w}_{\mathrm{Re}}(\mathbf{q}_2) d\hat{w}_{\mathrm{Im}}(\mathbf{q}_2) \cdots \\ &= \prod_{k(\mathbf{q}_k \cdot \mathbf{e}_y \geq 0)} \int_{-\infty}^{\infty} \int_{-\infty}^{\infty} \exp\left[-\frac{DL_0^2}{k_B T} q_k^4 (\hat{w}_{\mathrm{Re}}^2(\mathbf{q}_k) + \hat{w}_{\mathrm{Im}}^2(\mathbf{q}_k)) \right] d\hat{w}_{\mathrm{Re}}(\mathbf{q}_k) d\hat{w}_{\mathrm{Im}}(\mathbf{q}_k) \\ &= \prod_{k(\mathbf{q}_k \cdot \mathbf{e}_y \geq 0)} \left(\frac{\pi k_B T}{DL_0^2 q_k^4} \right) \end{aligned} \tag{15}$$

and Z_s is due to the in-plane modes (independent of the out-of-plane fluctuation). The range of each random variable in Eq. (15) has been taken to be from $-\infty$ to ∞ in order to obtain the analytical expression for the partition function. However, the formulation of the bending energy in Eq. (6) assumes moderately large deflection, requiring the fluctuation amplitude to be less than a fraction of its wavelength for each Fourier mode. Nevertheless, Eq. (15) offers a simple but reasonable approximation, considering that the exponential integrant decays rapidly with the variables. In other words, the large-amplitude fluctuations are statistically suppressed due to the large potential energy (hence low probability density).

With the probability density function in Eq. (13), the mean-square of each Fourier coefficient of the out-of-plane fluctuation can be calculated as

$$\langle |\hat{w}(\mathbf{q}_k)|^2 \rangle = \frac{1}{Z_b} \int_{-\infty}^{\infty} \cdots \int_{-\infty}^{\infty} |\hat{w}(\mathbf{q}_k)|^2 \exp\left(-\frac{U_b}{k_B T} \right) d\hat{w}_{\mathrm{Re}}(\mathbf{q}_1) d\hat{w}_{\mathrm{Im}}(\mathbf{q}_1) \cdots = \frac{k_B T}{DL_0^2 q_k^4}. \tag{16}$$

Alternatively, by the equi-partition theorem (Pathria, 1996), each independent harmonic term in Eq. (11) has an average energy of $k_B T/2$, namely

$$DL_0^2 q_k^4 \langle \hat{w}_{\mathrm{Re}}^2(\mathbf{q}_k) \rangle = DL_0^2 q_k^4 \langle \hat{w}_{\mathrm{Im}}^2(\mathbf{q}_k) \rangle = \frac{k_B T}{2}, \tag{17}$$

which leads to the same result as Eq. (16).

For each possible configuration, the mean-square amplitude of the out-of-plane fluctuation in the real space is

$$h^2 = \frac{1}{L_0^2} \iint_{\Omega} w^2(\mathbf{r}) d\Omega = \sum_k |\hat{w}(\mathbf{q}_k)|^2. \tag{18}$$

Therefore, the expectation value of the mean-square amplitude is

$$\langle h^2 \rangle = \sum_k \langle |\hat{w}(\mathbf{q}_k)|^2 \rangle = \frac{k_B T}{DL_0^2} \sum_k q_k^{-4}. \tag{19}$$

For the square-shaped membrane with periodic boundary conditions, the smallest possible wave number is: $q_{\min} = 2\pi/L_0$, which depends on the membrane size (L_0). The summation in Eq. (19) can then be written in a discrete

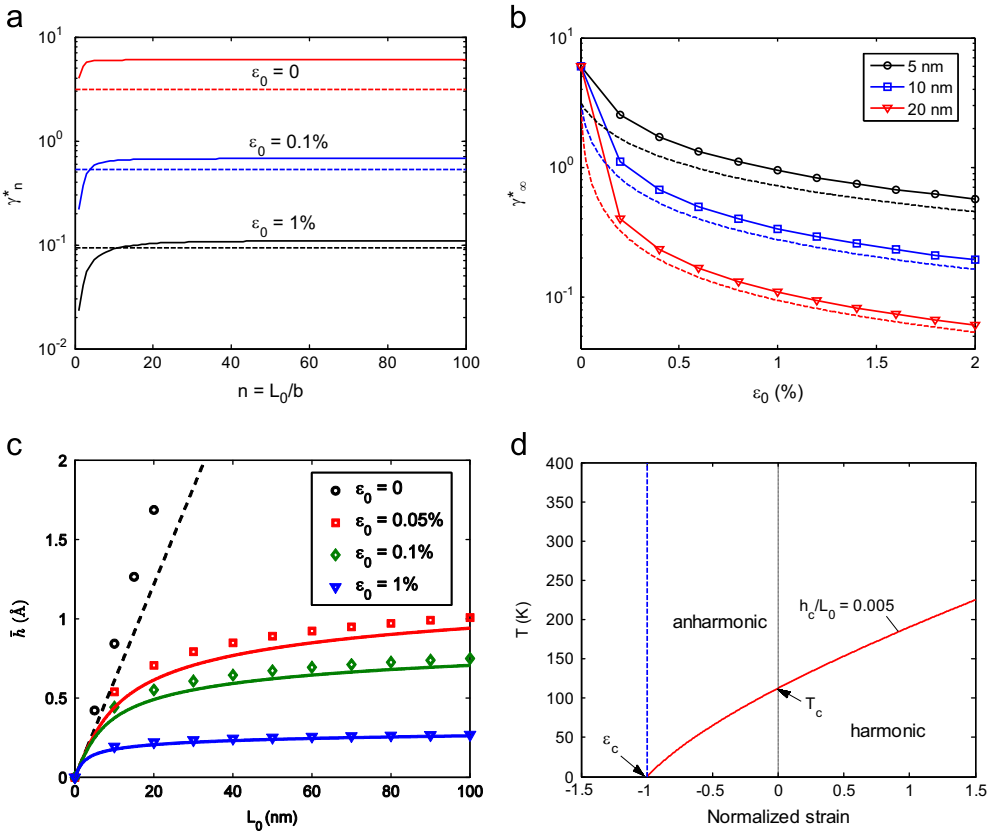

Fig. 1. (a) Convergence of the double-series summations in Eqs. (20) and (28), in comparison with the integral approximation (dashed lines) in Eqs. (21) and (29) for L_0=20 nm; (b) dependence of the coefficient γ^*_∞ on pre-strain for different membrane sizes (dashed lines by integration); (c) effect of pre-strain on RMS amplitude of out-of-plane thermal fluctuation at T=300 K by harmonic analysis (symbols by summation and lines by integration); (d) critical temperature as a function of the normalized pre-strain, $E^*L_0^2\varepsilon_0/4\pi^2D$, for the limit of harmonic analysis.

form as

$$\langle h^2\rangle = \frac{k_BT}{DL_0^2}\left(\frac{L_0}{2\pi}\right)^4 \sum_{\substack{i,j=-n \\ (i^2+j^2>0)}}^{n} (i^2+j^2)^{-2} = \frac{\gamma_n k_BT}{16\pi^4 D}L_0^2, \tag{20}$$

where γ_n is a dimensionless coefficient and $n = q_{\max}/q_{\min} = L_0/b$, with $q_{\max} = 2\pi/b$ being the largest possible wave number and b the smallest physically permissible length scale (e.g., a microscopic cut-off). Alternatively, Helfrich and Servuss (1984) suggested that the summation in Eq. (19) can be converted to an integral as a continuum approximation:

$$\langle h^2\rangle \approx \left(\frac{L_0}{2\pi}\right)^2 \int_{q_{\min}}^{q_{\max}} \left(\frac{k_BT}{DL_0^2}\frac{1}{q^4}\right) 2\pi q dq \approx \frac{k_BT}{16\pi^3 D}L_0^2, \tag{21}$$

where $L_0 \gg b$ has been assumed to simplify the result. A comparison between Eqs. (20) and (21) would lead to $\gamma_n \to \pi$ for $n \to \infty$. However, as shown in Fig. 1a, the discrete summation in Eq. (20) converges to a larger value, $\gamma_n \to 6.026$ (for zero strain), nearly twice of the integral approximation. The discrepancy results from the singular behavior of q_k^{-4} as $q_k \to 0$.

As a typical measure of surface roughness, the root-mean-square (RMS) amplitude of the out-of-plane fluctuation is obtained as

$$\bar{h} = \sqrt{\langle h^2\rangle} = L_0\sqrt{\frac{\gamma_n k_BT}{16\pi^4 D}}, \tag{22}$$

which scales linearly with the dimension (L_0) of the membrane. Similar results were obtained for thermal fluctuation of fluid membranes (Helfrich and Servuss, 1984). A slightly different derivation is presented here as an introduction to key concepts in statistical mechanics. Notably, the constant coefficient in Eq. (21) differs from that in Helfrich and Servuss (1984) by a factor of 4, since the integral is evaluated with different limits for the wave number, following the assumption of periodic boundary conditions. Moreover, the integral approximation in Eq. (21) is found to be inaccurate to evaluate the discrete summation in Eq. (20) for the amplitude of out-of-plane fluctuation, although the linear scaling ($\bar{h} \propto L_0$) is unaffected.

2.3. Effect of pre-strain

Next we consider thermal fluctuation of a graphene membrane subjected to a biaxial pre-strain ε_0, relative to the reference ground state. In addition to the bending energy, the in-plane stretching energy is

$$U_s = \iint_{\Omega} \left\{ E^*\varepsilon_0^2 + \frac{E^*\varepsilon_0}{2}\left[\left(\frac{\partial w}{\partial x}\right)^2 + \left(\frac{\partial w}{\partial y}\right)^2\right] + \frac{E^*}{8(1+\nu)}\left[\left(\frac{\partial w}{\partial x}\right)^2 + \left(\frac{\partial w}{\partial y}\right)^2\right]^2 \right\} dxdy. \tag{23}$$

With the pre-strain held as a constant, the out-of-plane deflection contributes to the local in-plane strain according to Eq. (1) and hence the strain energy density of the membrane in Eq. (4). In the presence of a non-zero pre-strain, the leading term of the contribution in Eq. (23) becomes quadratic. Again, we ignore the in-plane fluctuation and take Eq. (7) for the out-of-plane fluctuation. As a harmonic analysis, only the quadratic terms in Eq. (23) are retained, and the total stretching energy can be written in terms of the Fourier coefficients as

$$U_s = E^*\varepsilon_0^2 L_0^2 + E^*\varepsilon_0 L_0^2 \sum_{k(\mathbf{q}_k \cdot \mathbf{e}_y \geq 0)} q_k^2 \left[\hat{w}_{\mathrm{Re}}^2(\mathbf{q}_k) + \hat{w}_{\mathrm{Im}}^2(\mathbf{q}_k)\right]. \tag{24}$$

Along with the bending energy in Eq. (11), the total potential energy is

$$U = U_b + U_s = E^*\varepsilon_0^2 L_0^2 + L_0^2 \sum_{k(\mathbf{q}_k \cdot \mathbf{e}_y \geq 0)} (Dq_k^4 + E^*\varepsilon_0 q_k^2)\left[\hat{w}_{\mathrm{Re}}^2(\mathbf{q}_k) + \hat{w}_{\mathrm{Im}}^2(\mathbf{q}_k)\right]. \tag{25}$$

The partition function for the Boltzmann distribution in Eq. (13) is then obtained as a function of the pre-strain and temperature:

$$Z(\varepsilon_0, T) = \exp\left(-\frac{E^*\varepsilon_0^2 L_0^2}{k_B T}\right) \prod_{k(\mathbf{q}_k \cdot \mathbf{e}_y \geq 0)} \left[\left(1 + \frac{E^*\varepsilon_0}{Dq_k^2}\right)^{-1} \left(\frac{\pi k_B T}{DL_0^2 q_k^4}\right)\right]. \tag{26}$$

Following the same steps in the previous section, the expectation value of mean square amplitude of the out-of-plane fluctuation is obtained as

$$\langle h^2 \rangle = \frac{k_B T}{DL_0^2} \sum_k q_k^{-4} \left(1 + \frac{E^*\varepsilon_0}{Dq_k^2}\right)^{-1} = \frac{\gamma_n^* k_B T}{16\pi^4 D} L_0^2, \tag{27}$$

where

$$\gamma_n^* = \sum_{\substack{i,j=-n \\ i^2+j^2>0}}^{n} (i^2+j^2)^{-2} \left(1 + \frac{E^*\varepsilon_0 L_0^2}{4\pi^2 D} \frac{1}{i^2+j^2}\right)^{-1}. \tag{28}$$

Similar results were obtained by others for lipid membranes under tension (Helfrich and Servuss, 1984; Lomholt et al., 2011). As shown in Fig. 1a, the double-series summation in Eq. (28) converges for $n = L_0/b \to \infty$, i.e., $\gamma_n^* \to \gamma_\infty^*$, which depends on the pre-strain and the membrane size through the dimensionless group, $E^*\varepsilon_0 L_0^2/(4\pi^2 D)$. Again, a continuum approximation can be obtained by converting the summation in Eq. (27) to an integral (Helfrich and Servuss, 1984), which yields

$$\langle h^2 \rangle \approx \frac{k_B T}{4\pi E^*\varepsilon_0} \ln\left(1 + \frac{E^*\varepsilon_0 L_0^2}{4\pi^2 D}\right). \tag{29}$$

It can be shown that Eq. (29) reduces to Eq. (21) when the pre-strain $\varepsilon_0 \to 0$. As shown in Fig. 1b, the integral approximation underestimates the coefficient γ_∞^*, although the discrepancy is reduced with a positive pre-strain (tension).

As noted in Eq. (23), the presence of a pre-strain leads to a harmonic coupling between the out-of-plane fluctuation and in-plane stretching. This coupling introduces a length scale, $a = \sqrt{D/E^*}$. As a result, the RMS amplitude of the out-of-plane fluctuation is no longer scaling linearly with the membrane size, as shown in Fig. 1c. The out-of-plane thermal fluctuation is significantly suppressed by a positive pre-strain (tension), especially for relatively large membranes. On the other hand, when the pre-strain is negative (compression), it is interesting to note that the harmonic analysis predicts a singular behavior for the fluctuation amplitude as $\langle h^2 \rangle \to \infty$ for $\varepsilon_0 \to -q_k^2 D/E^*$ by Eq. (27), corresponding to a set of critical strains for buckling instability of the elastic membrane under compression. By Eq. (29), the fluctuation amplitude blows up at the first critical strain ($q_{\min} = 2\pi/L_0$):

$$\varepsilon_c = -\frac{4\pi^2 D}{E^* L_0^2}. \tag{30}$$

However, the buckling amplitude would remain finite beyond the critical strain if the higher order terms (anharmonic) in Eq. (23) are taken into account, a typical task for nonlinear post-buckling analysis left for future studies.

Since the harmonic analysis is limited to relatively small fluctuation amplitudes, a boundary line may be drawn in the temperature–strain panel as shown in Fig. 1d, where a critical value for the fluctuation amplitude, $h_c/L_0 = 0.005$, is assumed for illustrative purpose. In addition to the critical strain for buckling at $T=0$ K, a critical temperature at zero strain can be defined as

$$T_c = \frac{16\pi^4 D}{\gamma_n k_B}\left(\frac{h_c}{L_0}\right)^2. \tag{31}$$

Therefore, the harmonic analysis for the out-of-plane thermal fluctuation should be restricted to relatively low temperatures, with the critical temperature depending on the membrane size and pre-strain. For a monolayer graphene membrane, the critical strain for buckling is typically very small, around -2×10^{-4} for a membrane of size $L_0=10$ nm. Assuming $h_c/L_0 = 0.005$, the critical temperature at zero strain is about 112 K with $D = 1.5$ eV and $\gamma_n \approx 6.026$.

2.4. Nonlinear thermoelasticity of graphene

By classical theories of statistical mechanics and thermodynamics (Weiner, 2002), the microscopic partition function is related to the macroscopic Helmholtz free energy of the system as

$$A(\varepsilon_0, T) = -k_B T \ln Z(\varepsilon_0, T). \tag{32}$$

The equi-biaxial in-plane stress can then be obtained as a thermodynamic conjugate:

$$\sigma = \frac{1}{2L_0^2}\left(\frac{\partial A}{\partial \varepsilon_0}\right)_T. \tag{33}$$

By this definition, the stress has the same unit as the energy density (per unit area): J/m^2, or equivalently, N/m, so-called 2D stress as opposed to the conventional 3D stress.

With the partition function in Eq. (26), we obtain that

$$\sigma = E^*\varepsilon_0 + \frac{E^* k_B T}{2L_0^2}\sum_{k(\mathbf{q}_k\cdot\mathbf{e}_y\geq 0)} (Dq_k^2 + E^*\varepsilon_0)^{-1}, \tag{34}$$

where the first term is the biaxial stress in the ground state (no thermal fluctuation) and the second term is the entropic contribution, arising from the tendency of the graphene membrane to increase its entropy ($S=-\partial A/\partial T$) by out-of-plane fluctuation at a finite temperature. The entropic contribution to the stress can be calculated by summation over all Fourier components, namely

$$\tilde{\sigma} = \frac{E^* k_B T}{16\pi^2 D}\sum_{\substack{i,j=-n\\ i^2+j^2>0}}^{n}\left(i^2 + j^2 + \frac{E^*\varepsilon_0 L_0^2}{4\pi^2 D}\right)^{-1} = \frac{E^* k_B T}{16\pi^2 D}\xi_n. \tag{35}$$

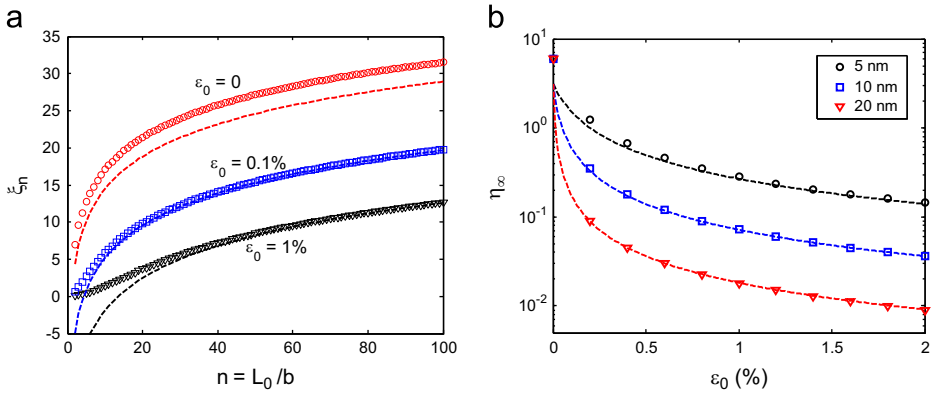

Fig. 2. (a) The coefficient ξ_n in Eq. (35) by summation (symbols) and integration (dashed lines) for $L_0=20$ nm; (b) the coefficient η_∞ in Eq. (36) as a function of pre-strain and membrane size (symbols by summation and lines by integration).

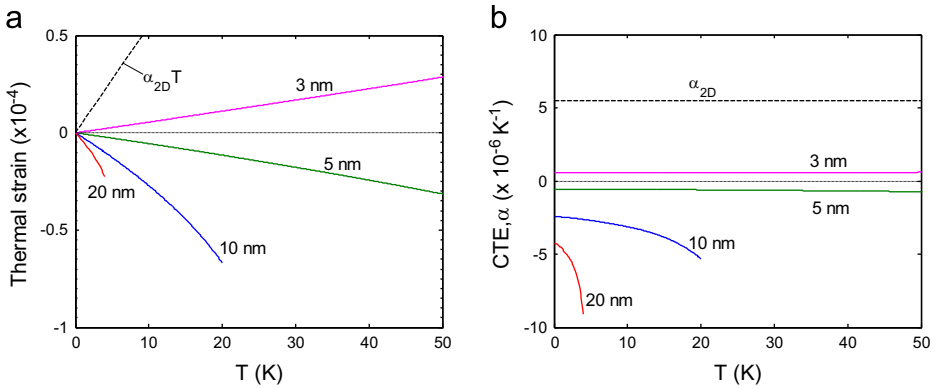

Fig. 3. (a) In-plane thermal strain predicted by the harmonic analysis for graphene membranes of different sizes; (b) effective coefficient of thermal expansion for graphene membranes predicted by the harmonic analysis.

It is found that this summation gives an unbounded stress for $n\to\infty$ even at zero strain (Fig. 2a). On the other hand, the corresponding elastic modulus is bounded as follows:

$$\tilde{E}^* = \frac{\partial\sigma}{\partial\varepsilon_0} = E^*\left[1-\frac{E^*k_BTL_0^2}{64\pi^4D^2}\sum_{\substack{i,j=-n\\ i^2+j^2>0}}^{n}\left(i^2+j^2+\frac{E^*\varepsilon_0L_0^2}{4\pi^2D}\right)^{-2}\right]\xrightarrow{n\to\infty}E^*\left[1-\frac{\eta_\infty E^*k_BTL_0^2}{64\pi^4D^2}\right] \tag{36}$$

where η_∞ is a function of the strain and the membrane size through the dimensionless group, $E^*\varepsilon_0L_0^2/(4\pi^2D)$, as shown in Fig. 2b. When $\varepsilon_0=0$, $\eta_\infty=\gamma_\infty=6.026$.

By converting the summations to integrals, the stress and modulus are obtained approximately as

$$\tilde{\sigma}\approx\frac{E^*k_BT}{16\pi D}\left[2\ln\left(\frac{L_0}{b}\right)-\ln\left(1+\frac{E^*L_0^2}{4\pi^2D}\varepsilon_0\right)\right], \tag{37}$$

$$\tilde{E}^*\approx E^*-\frac{E^*k_BT}{16\pi D}\left(\frac{4\pi^2D}{E^*L_0^2}+\varepsilon_0\right)^{-1}, \tag{38}$$

which agree closely with the summations except for $\varepsilon_0=0$ (Fig. 2). It is noted that a finite value of $\tilde{\sigma}$ depends on both the membrane size L_0 and the cutoff length b, while the latter is difficult to justify for the continuum model. In our calculations we have taken $b=4r_0=0.568$ nm, where $r_0=0.142$ nm is the equilibrium C–C bond length in graphene. Remarkably, independent of the cutoff, the effective modulus predicted by Eqs. (36) or (38) includes an entropic contribution due to the out-of-plane thermal fluctuation. As a result, the effective modulus of graphene depends on both the temperature and the membrane size. In particular, the harmonic analysis predicts that the biaxial modulus of graphene decreases linearly with temperature, hence a thermal softening effect. At zero strain, the modulus decreases with increasing membrane size (L_0). The size dependence becomes negligible when graphene is pre-stretched with $\varepsilon_0L_0^2\gg 4\pi^2D/E^*$. These predictions are further discussed in Section 4, in comparison with MD simulations.

In addition to the out-of-plane fluctuation, the in-plane thermal fluctuation, not considered explicitly in the present study, has an entropic contribution to the stress as well (Weiner, 2002). The total stress may be written approximately as

$$\sigma=E^*(\varepsilon_0-\alpha_{2D}T)+\tilde{\sigma}, \tag{39}$$

where α_{2D} is the 2D coefficient of thermal expansion (2D-CTE) resulting from anharmonic interactions among in-plane phonon modes when the out-of-plane modes are completely suppressed. As shown by MD simulations (Fig. 6b), the 2D-CTE of graphene is nearly a constant ($\alpha_{2D}\sim 5.51\times10^{-6}\,\mathrm{K}^{-1}$), independent of temperature or membrane size.

By setting the total stress to zero in Eq. (39), we obtain a nonlinear equation

$$\varepsilon_0+\frac{k_BT}{16\pi^2D}\sum_{\substack{i,j=-n\\ i^2+j^2>0}}^{n}\left(i^2+j^2+\frac{E^*\varepsilon_0L_0^2}{4\pi^2D}\right)^{-1}=\alpha_{2D}T, \tag{40}$$

which can be solved to predict the in-plane thermal strain, $\varepsilon_T=\varepsilon_0(\sigma=0)$, as a function of four dimensionless groups, $\alpha_{2D}T$, D/k_BT, $E^*L_0^2/D$, and n. Fig. 3a plots the thermal strain versus temperature for different membrane sizes. Without out-of-plane thermal fluctuation, the in-plane thermal strain increases linearly with temperature ($\sim\alpha_{2D}T$). The thermal strain is significantly reduced with out-of-plane thermal fluctuation. Since the amplitude of thermal fluctuation depends on the

membrane size, the reduction of thermal strain also depends on the membrane size. The thermal strain remains positive for a small membrane ($L_0=3$ nm), but becomes negative for larger membranes. By setting $\varepsilon_0=0$ in Eq. (40), the critical membrane size is predicted to be around 4.5 nm. Evidently, the in-plane contraction due to out-of-plane thermal fluctuation of the large membranes ($L_0>4.5$ nm) outweighs the positive expansion due to the in-plane modes, resulting in an effectively negative thermal expansion for graphene. Fig. 3b plots the effective in-plane CTE of graphene defined as

$$\alpha=\left(\frac{\partial\varepsilon_0}{\partial T}\right)_{\sigma=0}, \tag{41}$$

which depends on both the temperature and the membrane size due to the effect of out-of-plane fluctuation. We note that the harmonic approximation in the present analysis is limited to low temperatures for relatively large membranes. Beyond a critical temperature, no meaningful solution to Eq. (40) can be found, and anharmonic effects must be taken into account in order to predict the thermal expansion. Moreover, the harmonic approximation tends to overestimate the in-plane contraction, as discussed in Section 4.

2.5. Anharmonic effects

Theoretical studies of flexible membranes beyond the harmonic approximation have predicted that anharmonic coupling between bending and stretching modes could significantly suppress thermal fluctuation. Considering anharmonic effects with contributions from nonzero Gaussian curvatures, Nelson and Peliti (1987) predicted a power-law scaling for the mean amplitude of thermal fluctuation with respect to the linear dimension of a nearly flat elastic membrane: $\overline{h}\sim L^{\zeta}$, where ζ is called the roughness exponent: $\zeta=1$ by the harmonic approximation while $\zeta=0.5$ by Nelson and Peliti (1987). However, there is some uncertainty on the precise theoretical value of the roughness exponent, ranging from 0.5 to 0.775 for various membrane models (Lipowsky and Girardet, 1990; Abraham and Nelson, 1990; Gompper and Kroll, 1992; Le Doussal and Radzihovsky, 1992; Kownacki and Mouhanna, 2009). With nonlinear coupling between the out-of-plane fluctuation and in-plane displacements, analytical approximations and numerical treatments are required for anharmonic analysis, which remains a challenging subject. Moreover, the continuum membrane model with energy functionals such as Eqs. (6) and (23) are limited to relatively small fluctuation amplitude and in-plane strain. These limitations can be lifted by discrete atomistic models of the membrane. By atomistic MC and MD simulations, Los et al. (2009) found the roughness exponent to be around 0.575 for graphene. MD simulations by Abedpour et al. (2007) predicted a temperature dependent roughness exponent in the range $0.6<\zeta<0.74$ for $T=0$–700 K. The anharmonic effect on thermal fluctuation is expected to have a profound influence on the thermomechanical properties of graphene. As predicted by atomistic modeling and simulations (Zakharchenko et al., 2009; Chen and Chrzan, 2011), the elastic modulus of graphene depends on the temperature and the in-plane thermal expansion changes from negative to positive as the temperature increases. In the present study, by comparing numerical results from MD simulations with theoretical predictions under the harmonic approximation, we emphasize the intimate relationship between thermal rippling and thermoelasticity of graphene with both harmonic and anharmonic effects. Moreover, the statistical nature of thermal rippling renders an entropic contribution to thermoelasticity; similar entropic effects have been well known for many other materials, including isolated molecular chains (Marko and Siggia, 1995), biological membranes (Safran, 1994), and molecular networks (Treloar, 1958; Su and Purohit, 2012).

3. Molecular dynamics simulation

We perform MD simulations of monolayer graphene using LAMMPS, an open source code (Plimpton, 1995). The second-generation reactive empirical bond-order (REBO) potential (Brenner et al., 2002) is used for the multibody C–C interactions

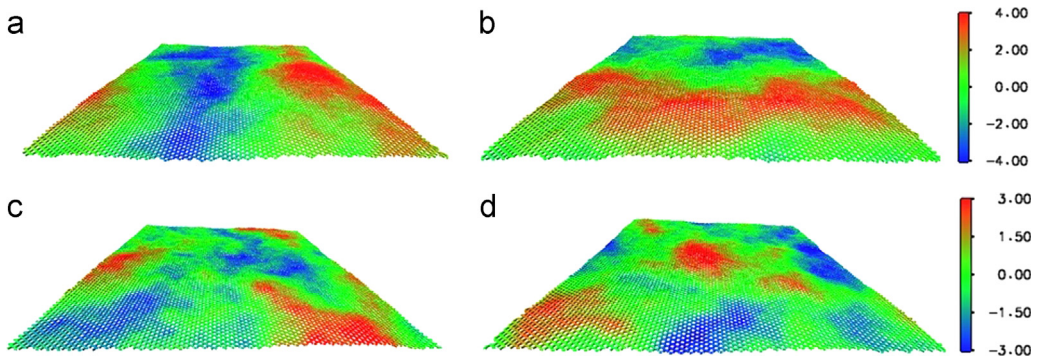

Fig. 4. Snapshots of thermal rippling of a graphene membrane by MD simulations with $L_0=20$ nm and $T=300$ K. (a) and (b) for NPT with zero stress; (c) and (d) for NVT with zero strain. Color bars show out-of-plane deflection of atoms in Å. (For interpretation of the references to color in this figure legend, the reader is referred to the web version of this article.)

in graphene. Square-shaped graphene membranes of different linear dimensions are simulated at finite temperatures with periodic boundary conditions. The temperature is controlled by a Nose-Hoover thermostat. Each simulation runs up to 40 ns (time step: 1 fs), with the first 10 ns for the system to equilibrate and the subsequent 30 ns for calculations of the time-averaged quantities. The time integration scheme closely follows the time-reversible measure-preserving Verlet and rRESPA integrators derived by Tuckerman et al (1992). The statistical errors are estimated by fifteen different sets of data, each over a time interval of 2 ns. To simulate monolayer graphene without interlayer interactions, relatively thick simulation boxes are used (thickness >20 nm). VMD, an open source visualization package (Humphrey et al., 1996), was used to generate snapshots of graphene membranes (Fig. 4).

MD simulations with both constant pressure (NPT) and constant volume (NVT) ensembles are performed. In NPT simulations, the dimensions of the simulation box are allowed to change to maintain a constant pressure (or stress). In particular, we are interested in zero-pressure (or zero-stress) NPT simulations for freestanding graphene membranes, with which the change of the in-plane dimension is calculated as a function of temperature to predict the in-plane CTE of graphene, namely

$$\alpha(T, L_0) = \frac{1}{L_0}\left(\frac{\partial \langle L\rangle_t}{\partial T}\right), \tag{42}$$

where L_0 is the linear dimension of the graphene membrane in the ground state ($T=0$ K) and $\langle L\rangle_t$ denotes time average of the linear dimension at a finite temperature. On the other hand, the NVT ensemble is used to simulate graphene subjected to a pre-strain (ε_0). In such simulations, the dimensions of the simulation box are fixed as $L=L_0(1+\varepsilon_0)$, while the in-plane reaction stress is evaluated as a function of the pre-strain and temperature by time-averaged virial stress (Admal and Tadmor, 2010):

$$\boldsymbol{\sigma} = -\left\langle \frac{1}{2L^2}\sum_{\substack{i,j\\ i\neq j}} \mathbf{F}_{ij}\otimes(\mathbf{r}_i-\mathbf{r}_j) + \frac{1}{L^2}\sum_i m_i\mathbf{v}_i\otimes\mathbf{v}_i\right\rangle_t \tag{43}$$

where $\mathbf{F}_{ij}$ is the interatomic force between two atoms (i and j), $\mathbf{r}_i$ is the position vector of i-th atom, $\mathbf{v}_i$ is the velocity vector, m_i is the atomic mass, and $\langle\cdot\rangle_t$ denotes time average of the enclosed quantity. The virial formula is modified to yield the 2D stress for graphene, consistent with the definition of stress in Eq. (33).

In both NPT and NVT simulations, the mean amplitude of the out-of-plane thermal fluctuation is calculated by a time averaged RMS, namely

$$\overline{h} = \sqrt{\left\langle \sum_{i=1}^{N}\frac{w_i^2}{N}\right\rangle_t}, \tag{44}$$

where N is the total number of atoms and w_i is the out-of-plane displacement of i-th atom. Based on the ergodic hypothesis (Weiner, 2002), the time average (over a sufficiently long period) from MD simulation is equivalent to the ensemble average in statistical mechanics. Consequently, the numerical results from MD simulations can be compared directly with the predictions based on statistical mechanics.

Moreover, we perform special 2D-MD simulations to study the behavior of graphene membranes in the absence of out-of-plane thermal fluctuation. For a 2D-MD simulation, the out-of-plane components of velocities and forces are zeroed out for all atoms in every time step. As a result, the graphene membrane remains perfectly flat, but with in-plane fluctuations. It is found that the computational cost and statistical error of 2D-MD are drastically reduced in comparison with regular MD. Each simulation is sufficiently equilibrated by running to 5 ns with a time step of 1 fs. Through these 2D-MD simulations, we obtain a 2D-CTE ($\alpha_{2D}\sim 5.51\times 10^{-6}\,\mathrm{K}^{-1}$) and biaxial stress-strain relation without out-of-plane thermal fluctuation. A comparison with the regular MD simulations would then reveal the effects of out-of-plane thermal fluctuation.

4. Results and discussion

4.1. Thermal rippling

Fig. 4 shows snapshots of a graphene membrane from MD simulations. The out-of-plane thermal fluctuation leads to dynamic thermal rippling under both NPT and NVT conditions. The time averaged RMS amplitude of thermal rippling is plotted in Fig. 5, as a function of temperature and membrane size. The rippling amplitude under the zero-stress NPT condition compares closely with previous studies (Fasolino et al., 2007; Los et al., 2009). Compared to the prediction by the harmonic analysis, the rippling amplitude is considerably lower, suggesting significant anharmonic effect, especially at high temperatures and for large membranes. Under the zero-strain NVT condition, the rippling amplitude is even lower. This can be understood as a result of the reactive tensile stress that is required to hold the in-plane dimension of the membrane, as discussed further in Section 4.2. A common assumption in the studies of flexible membranes is inextensibility of the in-plane dimension (Helfrich and Servuss, 1984). Such an assumption would erroneously predict zero out-of-plane

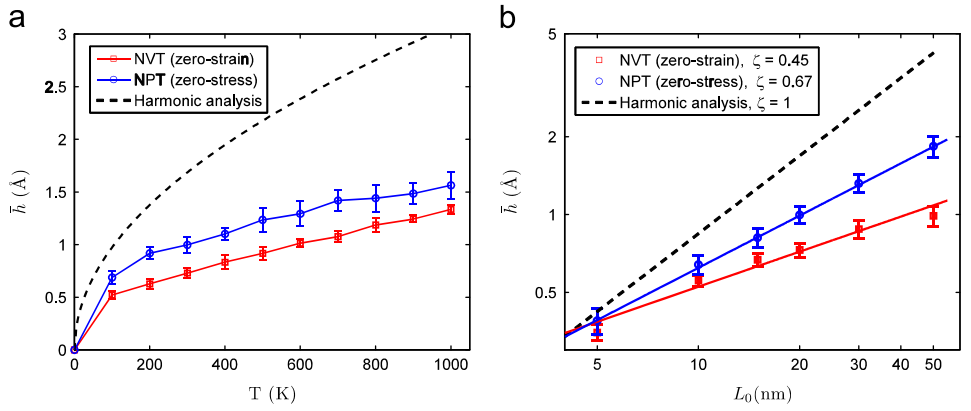

Fig. 5. (a) RMS amplitude of thermal rippling of a graphene membrane (L_0=20 nm) as a function of temperature, from MD simulations under zero-stress NPT and zero-strain NVT conditions. (b) Rippling amplitude as a function of membrane size at T=300 K, fitted by the scaling law, $\bar{h} \propto L_0^{\zeta}$, with different roughness exponents for NPT and NVT ensembles.

fluctuation under the zero-strain condition. Evidently, in-plane extension is inevitable at a finite temperature despite the high in-plane stiffness of graphene.

In Fig. 5b, the rippling amplitude as a function of the membrane size is fitted by the power law, $\bar{h} \sim L^{\zeta}$, which yields two roughness exponents, $\zeta = 0.67$ for NPT (zero stress) and $\zeta = 0.45$ for NVT (zero strain), both at T=300 K. The NPT roughness exponent agrees well with a previous study (Abedpour et al., 2007), which is also close to the theoretical predictions for other flexible membranes (Lipowsky and Girardet, 1990; Abraham and Nelson, 1990; Gompper and Kroll, 1992; Le Doussal and Radzihovsky, 1992; Kownacki and Mouhanna, 2009). The lower roughness exponent under the zero-strain NVT condition suggests that the scaling law sensitively depends on the boundary constraint. As predicted by the harmonic analysis in Fig. 1c and MD simulations (Fig. 7a), a small positive pre-strain could suppress rippling amplitude considerably and result in very different scaling behavior. Experimentally, when a graphene membrane is suspended over a hole or trench (Meyer et al., 2007; Bangert et al., 2009; Zan et al., 2012), a positive pre-strain or tension is likely imposed due to the adhesive interaction between graphene and the side wall of the hole/trench (Lee et al., 2008; Bunch, et al., 2008; Lu and Dunn, 2010). Furthermore, change of temperature would lead to thermal stress in graphene due to thermal expansion mismatch. While a tensile thermal stress would suppress thermal rippling, a compressive thermal stress could lead to static rippling by buckling instability (Bao et al., 2009). Therefore, the dependence of rippling amplitude on temperature could be coupled with thermal expansion induced stress in suspended graphene (Kirilenko et al., 2011), further discussed in Section 4.3.

4.2. Thermal expansion

Thermal expansion of a freestanding graphene membrane is studied by MD simulations under the zero-stress NPT condition. As shown in Fig. 6a, the macroscopic in-plane strain components are calculated by time averaging at different temperatures for different membrane sizes, i.e., $\bar{\varepsilon}_x = \langle L_x \rangle_t / L_0 - 1$ and $\bar{\varepsilon}_y = \langle L_y \rangle_t / L_0 - 1$, where L_0 is the in-plane dimension of the square-shaped membrane in the ground state (T=0 K) whilst L_x and L_y are projected in-plane dimensions at a finite temperature. The two strain components are nearly identical in all cases, suggesting transversely isotropic thermal expansion of graphene. Similar to the prediction by the harmonic analysis (Fig. 3a), the thermal strain becomes increasingly negative as the membrane size increases, which has been attributed to the in-plane contraction as a result of out-of-plane thermal fluctuation. Indeed, by suppressing out-of-plane fluctuation, 2D-MD simulations predict linear, positive thermal expansion (Fig. 6b), independent of the membrane size. A positive 2D-CTE is obtained as $\alpha_{2D} = 5.51 \times 10^{-6}\ \mathrm{K}^{-1}$, which remains constant up to T=1000 K. Such a positive thermal expansion can be understood as a result of anharmonic interactions among in-plane phonon modes (Weiner, 2002). By subtracting the in-plane expansion from the total thermal strain, i.e., $\tilde{\varepsilon} = \bar{\varepsilon} - \alpha_{2D} T$, we obtain the in-plane contraction due to out-of-plane fluctuation, which depends on the temperature and membrane size (Fig. 6b). In particular, while the in-plane contraction increases monotonically with increasing temperature, the rate of increase is slowed down at high temperatures due to the anharmonic effect on thermal rippling. Consequently, the total thermal strain turns to become increasingly positive (or less negative) at high temperatures. The competition between the two effects (in-plane and out-of-plane modes) on thermal expansion of graphene leads to a non-monotonic behavior of thermal strain (Fig. 6a), except for very small membrane size (e.g., 3 nm). A previous study based on quasi-harmonic approximation (QHA) predicted monotonic decreasing of the in-plane lattice parameter of graphene (Mounet and Marzari, 2005), which may have underestimated the anharmonic effects and thus overestimated the in-plane contraction at high temperatures. More recently, atomistic MC simulations by Zakharchenko et al. (2009) showed non-monotonic change of the in-plane lattice parameter of graphene, similar to the thermal strain in Fig. 6a.

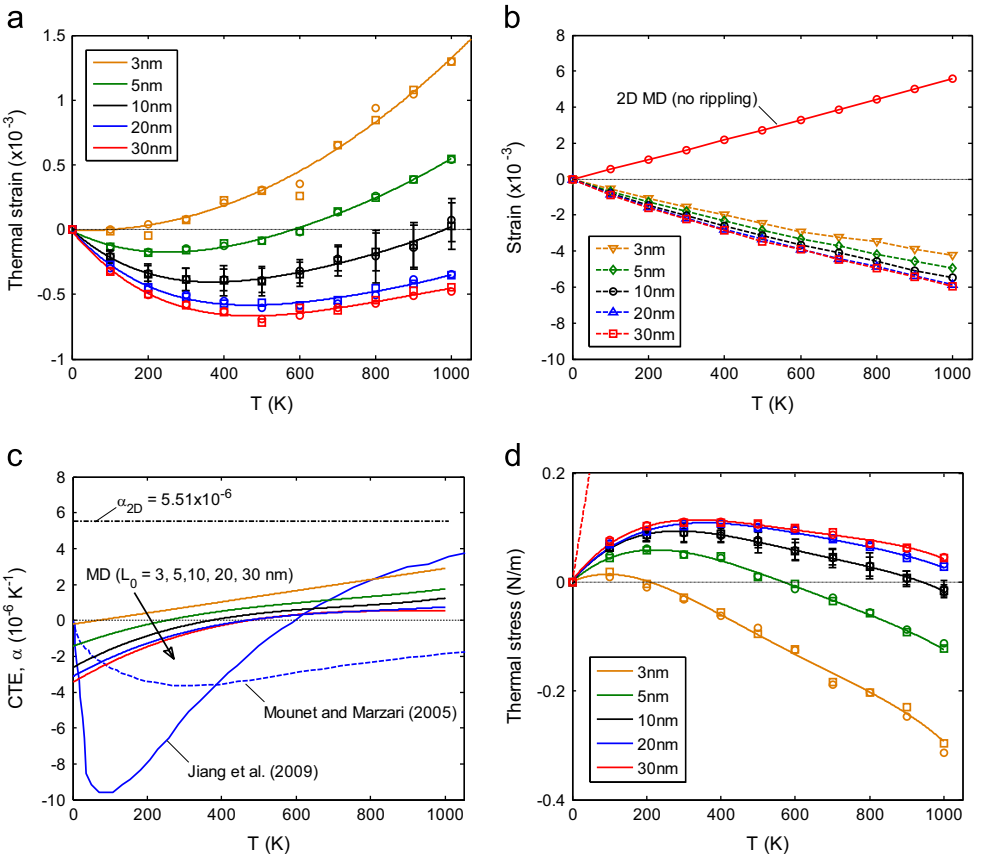

Fig. 6. (a) In-plane thermal strain of graphene by MD simulations under the zero-stress NPT condition, as a function of temperature for different membrane sizes. Squares and circles are for strain components in the armchair and zigzag directions, respectively; error bars are shown for $L_0=10$ nm only; solid curves are fourth-order polynomial fittings. (b) Linear, positive thermal expansion of graphene by 2D-MD simulations and the in-plane contraction strain due to out-of-plane thermal fluctuation. (c) Coefficient of thermal expansion of graphene as a function of temperature, comparing MD simulations with two previous studies. (d) In-plane thermal stress of graphene under zero-strain NVT condition, where the red dashed line shows the prediction by the harmonic analysis for $L_0=30$ nm.

The nonlinear dependence of the thermal strain on temperature is fitted by a polynomial function (solid lines in Fig. 6a), with which the in-plane CTE of graphene is calculated as a function of temperature for different membrane sizes (Fig. 6c). For a relatively large membrane, the calculated CTE is negative below a critical temperature but becomes positive at higher temperatures. The critical temperature varies from around 100 to 500 K for the membrane size ranging from 3 to 30 nm. The transition from negative to positive CTE can also be understood as a result of the competition between the in-plane and out-of-plane modes. In comparison, similar transition to a positive CTE was predicted by Jiang et al. (2009) using a non-equilibrium Green's function method, while the CTE predicted by Mounet and Marzari (2005) remains negative up to $T=2000$ K. Experimentally, Bao et al. (2009) reported a transition temperature at around 350 K, close to the present MD results. While quantitative discrepancies remain to be resolved by more accurate experimental measurements, the prediction for the negative-to-positive transition of CTE is theoretically plausible for graphene, considering the anharmonic effect on thermal rippling. Such transition of CTE has been also predicted and confirmed experimentally for graphite (Mounet and Marzari., 2005), where the out-of-plane thermal fluctuation is confined by interlayer van der Waals interactions.

We note that the in-plane CTEs of graphene obtained from MD simulations increase monotonically with temperature. In contrast, decreasing of CTE was predicted by both QHA (Mounet and Marzari, 2005) and Green's function method (Jiang et al., 2009). This discrepancy is largely attributed to the inaccuracy of MD simulations at very low temperatures ($T<100$ K), when the dimensional change is relatively small and thus the thermal strain cannot be accurately determined. Moreover, it is known in solid state physics that quantum effect dominates the low-temperature behavior for specific heat and thermal expansion (Ashcroft and Mermin, 1976), which is not accounted for in the classical MD simulations. Interestingly, the harmonic analysis in Section 2 does predict decreasing CTEs for relatively large membranes (Fig. 3b), despite the limited temperature range. However, the coincidence may not be physically justifiable without taking into account the quantum effect at low temperatures.

With a negative CTE below the transition temperature, a tensile stress is expected for a graphene membrane when its in-plane dimension is fixed. Indeed, as shown in Fig. 6d, the in-plane reaction stress calculated from MD simulations under the zero-strain NVT condition is positive at low temperatures and reaches a peak at around the transition temperature. However, since the amplitude of thermal rippling is lower under the zero-strain condition (Fig. 5a), the CTE of graphene obtained under the zero-stress NPT condition cannot be used directly to predict the thermal stress here. On the other hand, by setting $\varepsilon_0 = 0$ in Eq. (39), the harmonic analysis would predict the thermal stress to be linearly dependent on temperature (dashed line in Fig. 6d), overestimating the stress considerably. Therefore, the anharmonic effect on thermal rippling of graphene is intricately coupled with thermal expansion and thermal stress, resulting in a generally nonlinear thermo-mechanical behavior of graphene.

4.3. Thermoelasticity

Assuming linear elasticity in the ground state ($T=0$ K), a nonlinear stress–strain behavior is predicted at a finite temperature ($T>0$ K) by the statistical mechanics approach in Section 2 (Eq. 39), including an entropic contribution to the stress due to out-of-plane thermal fluctuation. This behavior is in contrast to the classical theory of linear thermoelasticity, where the total strain is taken as linear superposition of elastic strain and thermal expansion. For graphene, however, the thermal expansion cannot be determined independently from elastic strain (or stress), largely due to thermal rippling and its dependence on strain (or stress) as discussed in Section 4.2. While the harmonic analysis in Section 2 is limited for its own applicability, the nonlinear thermoelasticity of graphene is confirmed by MD simulations beyond the harmonic regime. By imposing an equi-biaxial in-plane strain under the NVT condition, the corresponding stress in graphene is calculated as a function of the strain and temperature. Meanwhile, the RMS amplitude of rippling is also calculated to show its effect on the stress–strain relation. As shown in Fig. 7a for a graphene membrane with $L_0=20$ nm at 300 K, the ripple amplitude decreases with increasing strain. Compared to the prediction by the harmonic analysis, Eq. (27), the rippling amplitude from MD is considerably lower around zero strain, due to the anharmonic effect as discussed in Section 4.1. With increasing positive strain, the MD results compare closely with the harmonic prediction, suggesting that the anharmonic effect is suppressed by the tensile strain. Fig. 7b shows the stress–strain curve for the same membrane. For comparison, a stress–strain curve is also obtained from 2D-MD simulations in absence of any out-of-plane fluctuation. The difference between the

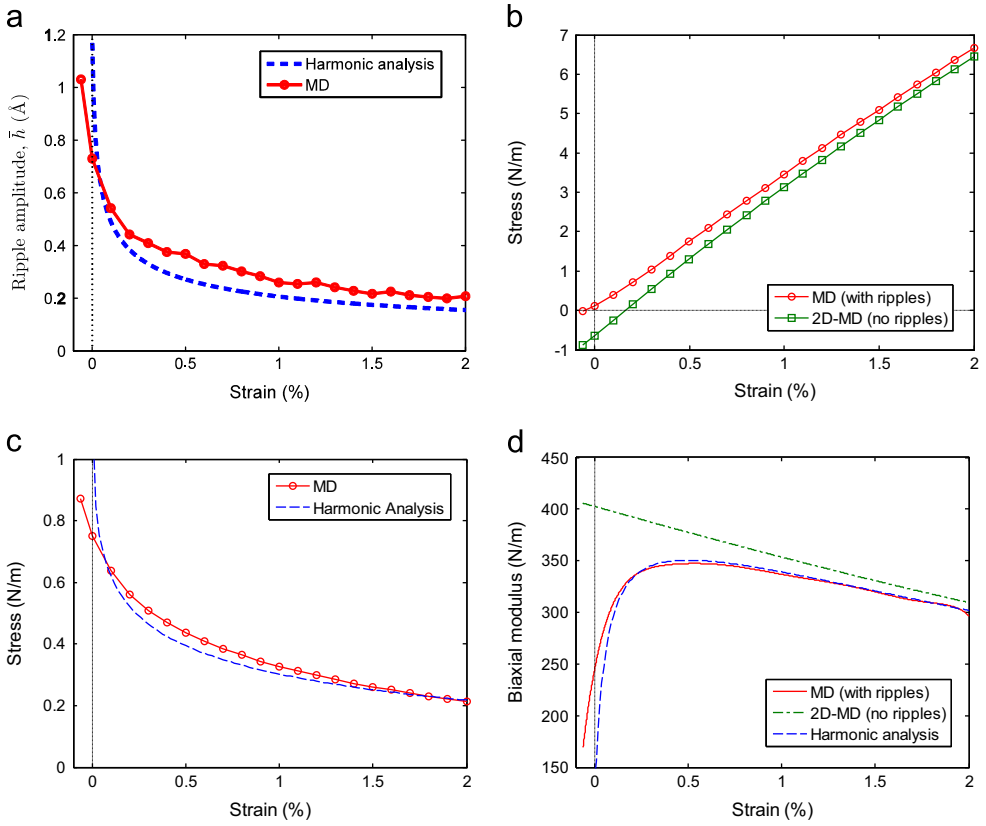

Fig. 7. (a) RMS amplitude of rippling as a function of biaxial strain for a graphene membrane ($L_0=20$ nm) at $T=300$ K, comparing the results from MD simulations with prediction by the harmonic analysis. (b) Stress–strain curves from MD simulations with and without rippling. (c) Entropic contribution to the stress as a function of strain. (d) Biaxial modulus as a function of strain.

two stress–strain curves is attributed to the entropic contribution from rippling, as shown in Fig. 7c, in comparison with the prediction in Eq. (35) by the harmonic analysis. Similar to the rippling amplitude in Fig. 7a, the harmonic analysis overestimates the entropic contribution at zero strain, but becomes reasonably good with a positive strain.

With the stress–strain curves in Fig. 7b, the tangent biaxial modulus of graphene is calculated by numerical differentiation as shown in Fig. 7d. Even without out-of-plane fluctuation, the biaxial modulus obtained from 2D-MD simulations is not a constant, decreasing with increasing strain. Such a nonlinear elastic behavior has been predicted previously by both DFT (Wei et al., 2009) and MM calculations (Lu and Huang, 2009; Lu et al., 2011) at $T=0$ K, which is nearly independent of temperature and hence considered intrinsic. With out-of-plane fluctuation, the elastic modulus is significantly lower at small strain. As predicted by the harmonic analysis in Section 2.4, the out-of-plane fluctuation reduces the effective elastic modulus in Eqs. (36) or (38). The amount of reduction, $\Delta E^* = E^* - \tilde{E}^*$, decreases with increasing strain, which is a result of decreasing ripple amplitude. Consequently, the elastic modulus first increases with strain (i.e., strain stiffening) as the ripple amplitude decreases. As the rippling effect diminishes with further increasing of strain ($>0.5\%$), the intrinsic nonlinear elasticity takes over so that the elastic modulus decreases, following closely the results from 2D-MD simulations or the ground-state behavior. Therefore, the nonlinear elasticity of graphene at a finite temperature results from two physical origins, one intrinsic (independent of temperature) and the other owing to out-of-plane fluctuation for $T>0$ K. The competition between the two effects results in a non-monotonic dependence of the tangent elastic modulus of graphene on strain (Fig. 7d), even at the infinitesimal strain level. For comparison, the elastic modulus predicted by the harmonic analysis is plotted in Fig. 7d, using the elastic modulus from 2D-MD in place of E^* in Eq. (36). Evidently, the modified harmonic prediction agrees well with the MD results for a relatively large strain ($>0.5\%$), but less so near zero strain.

The effect of out-of-plane fluctuation leads to temperature and size-dependent elastic properties for graphene. As shown in Fig. 8a, the stress–strain curves of a graphene membrane with $L_0=20$ nm are obtained from MD simulations at different temperatures at around zero strain (relative to the ground state). At a very low temperature (e.g., $T=10$ K), the stress–strain

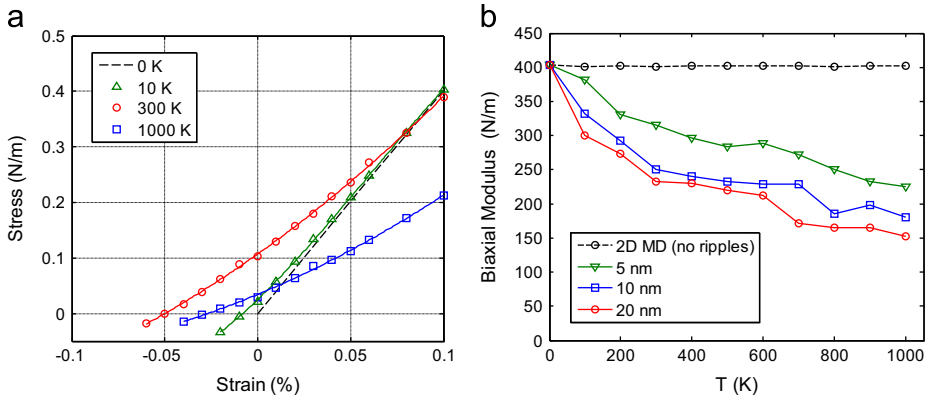

Fig. 8. (a) Biaxial stress–strain curves around zero strain for a graphene membrane with $L_0=20$ nm, obtained from MD simulations at three different temperatures, in comparison with the ground-state behavior at $T=0$ K from static MM calculations. (b) Tangent biaxial modulus at zero strain as a function of temperature for different membrane sizes.

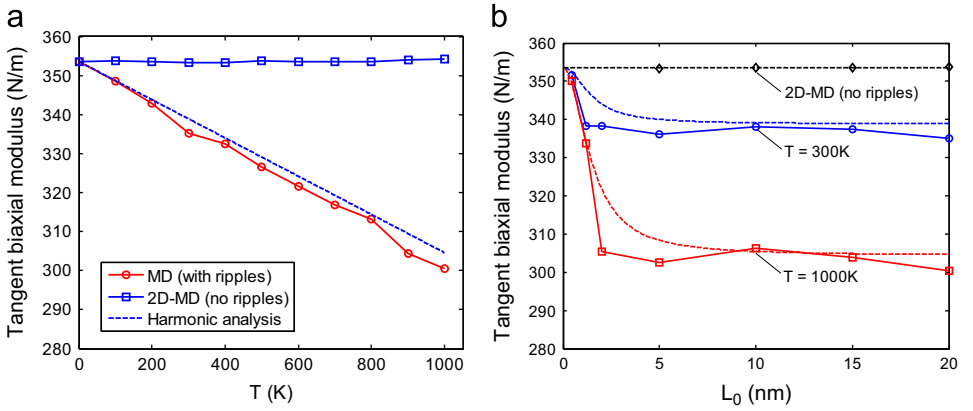

Fig. 9. (a) Tangent biaxial modulus at 1% strain as a function of temperature for a graphene membrane with $L_0=20$ nm, obtained from MD and 2D-MD simulations, in comparison with the harmonic analysis. (b) Tangent biaxial modulus at 1% strain as a function of membrane size at $T=300$ and 1000 K.

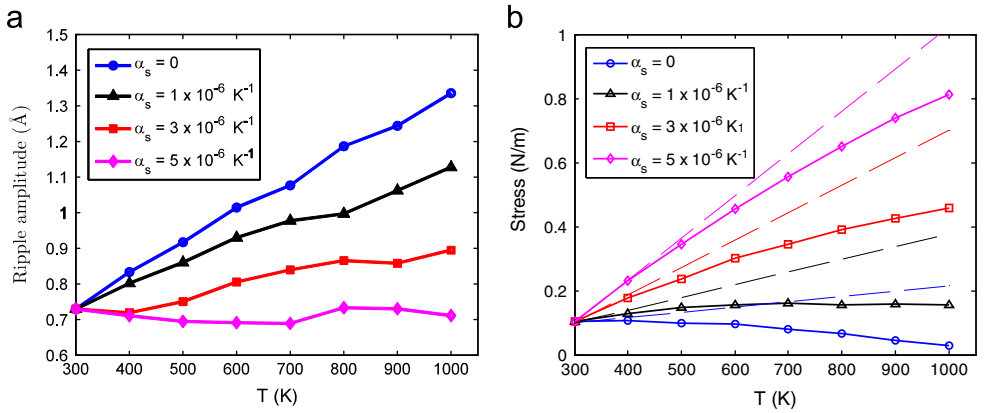

Fig. 10. (a) RMS amplitude of rippling obtained from MD simulations as a function of a temperature for a 20 nm graphene membrane suspended on a substrate with different CTEs. (b) Biaxial stress versus temperature. The thin dashed lines in (b) are linear prediction of the stress using the properties of graphene at $T=300$ K ($\alpha_g=-0.7\times10^{-6}$ K^{-1} and $\tilde{E}^*=232$ N/m).

behavior is close to the ground-state behavior at $T=0$ K, which can be obtained from the static MM simulation (Lu and Huang, 2009). As the temperature increases, the slope of the stress–strain curve decreases, indicating thermal softening in the elastic modulus. Fig. 8b plots the tangent modulus at zero strain as a function of temperature for three different membrane sizes. For comparison, the tangent modulus obtained from 2D-MD is also plotted, showing essentially no temperature dependence with $E^*=403.0\ N/m$, in close agreement with DFT calculations ($E^*\sim406$ N/m) (Kudin et al., 2001; Wei et al., 2009). It is well known that elastic modulus of a crystalline solid is in general temperature dependent and in particular, linear temperature dependence has been predicted under the harmonic approximation (Weiner, 2002). Similarly for graphene, the harmonic analysis in Section 2 predicts linear thermal softening of the elastic modulus in Eqs. (36) or (38). However, with significant anharmonic effect at zero strain, a nonlinear temperature dependence is predicted for the elastic modulus of graphene (Fig. 8b). Moreover, the elastic modulus of graphene is size dependent: lower modulus for larger membrane size due to more significant rippling.

The tangent elastic modulus of graphene depends on strain (Fig. 7d). Subject to a moderately large tensile strain ($\sim$1%), the anharmonic effect on rippling is significantly reduced, and as a result the harmonic analysis could be used to predict the temperature/size-dependence of elastic modulus. As shown in Fig. 9a, the tangent biaxial modulus at 1% strain decreases with increasing temperature for a graphene membrane with $L_0=20$ nm, in close agreement with the linear dependence predicted by the harmonic analysis. Note that, due to the intrinsic nonlinear elasticity, the biaxial modulus in the ground state (E^*) has to be adjusted to the value at 1% strain ($\sim$353.6 N/m) for the harmonic analysis. Again, 2D-MD simulations predict a biaxial modulus independent of temperature. The size dependence of the tangent modulus at 1% strain is shown in Fig. 9b. The elastic modulus drops rapidly from the ground-state value (353.6 N/m) to a constant level for $L_0>2$ nm at each temperature. As predicted by the harmonic analysis, the size dependence becomes negligible when $\varepsilon_0 L_0^2 \gg 4\pi^2 D/E^*$ or $L_0 \gg 1.6$ nm for $\varepsilon_0=1\%$.

Finally, as one application, we consider a graphene membrane suspended over a square hole on a substrate. As the temperature increases from 300 K to 1000 K, thermal expansion of the substrate imposes a positive equi-biaxial strain to the membrane, $\varepsilon=\alpha_s\Delta T$, where α_s is the CTE of the substrate (assumed to be a constant). As a result, rippling of the suspended graphene membrane is subjected to two competing effects: increasing temperature and strain. As shown in Fig. 10a, by MD simulations, the change of rippling amplitude for the suspended graphene depends on the CTE of the substrate. With a relatively large substrate CTE, the ripple amplitude decreases with increasing temperature, in contrast to the cases with either zero strain or zero stress (Fig. 5a). Experimental evidence for decreasing membrane roughness with increasing temperature has been reported by Kirilenko et al. (2011). Moreover, an equi-biaxial stress is induced in the suspended graphene membrane due to mismatch in thermal expansion. The stress changes with temperature as follows:

$$\frac{d\sigma}{dT}=\tilde{E}^*(\alpha_s-\alpha_g). \tag{45}$$

For the graphene membrane, both the CTE (α_g) and the biaxial modulus ($\tilde{E}^*$) depend on the temperature and stress. Therefore, integration of Eq. (45) would in general lead to a nonlinear dependence of the thermal stress on temperature. The results from MD simulations are shown in Fig. 10b. Assuming zero strain (relative to the ground state) at $T=300$ K, the membrane is subjected to an initial tensile stress of 0.1 N/m. Under the zero strain condition ($\alpha_s=0$), the stress decreases slightly as the temperature increases, because the CTE of graphene becomes positive at high temperatures (Fig. 6c). With $\alpha_s>0$, the stress increases with temperature nonlinearly. On the other hand, using the thermomechanical properties of graphene at 300 K in Eq. (45), the linear prediction (dashed lines) considerably overestimates the stress at high temperatures (>400 K).

5. Summary

We present a statistical mechanics analysis and molecular dynamics simulations of monolayer graphene membranes under a variety of thermomechanical conditions. Comparison between the two approaches highlights significant anharmonic effects on rippling and thermoelasticity of graphene. The main findings are summarized as follows.

- The amplitude of thermal rippling depends nonlinearly on the graphene membrane size due to anharmonic interactions between bending and stretching modes. Different roughness exponents are predicted for a power-law scaling under zero stress and zero strain conditions. However, a small positive pre-strain could suppress rippling amplitude considerably and result in very different scaling behavior.
- Negative in-plane thermal expansion of graphene is predicted at relatively low temperatures, with a transition to positive thermal expansion at high temperatures. The transition is a result of two competing effects: positive thermal expansion due to in-plane modes and negative expansion due to out-of-plane fluctuation. The latter is suppressed by the anharmonic effect at high temperatures.
- The biaxial stress–strain relation of graphene is generally nonlinear at a finite temperature, even for an infinitesimal strain. It is found that the tangent biaxial modulus of graphene depends on strain non-monotonically, with strain stiffening followed by intrinsic softening. With an entropic contribution due to rippling, the elastic modulus of graphene depends on both temperature and membrane size.
- Finally, for a suspended graphene membrane, the ripple amplitude may increase or decrease with increasing temperature, depending on the coefficient of thermal expansion of the substrate.

Acknowledgments

The authors gratefully acknowledge financial support of this work by the National Science Foundation through Grant nos. CMMI-0926851 and CMMI-1130261. The authors thank Dr. L.B. Freund of University of Illinois at Urbana-Champaign for helpful discussions. The authors acknowledge the Texas Advanced Computing Center (TACC) at the University of Texas at Austin for providing HPC resources that have contributed to the research results reported within this paper.

References

Abedpour, N., Neek-Amal, M., Asgari, R., Shahbazi, F., Nafari, N., Tabar, M.R.R., 2007. Roughness of undoped graphene and its short-range induced gauge field. Phys. Rev. B 76, 195407.
Abraham, F.F., Nelson, D.R., 1990. Fluctuations in the flat and collapsed phases of polymerized membranes. J. Phys. (Paris) 51 (23), 2653–2672.
Admal, N.C., Tadmor, E.B., 2010. A unified interpretation of stress in molecular systems. J. Elast. 100 (1), 63–143.
Arroyo, M., Belytschko, T., 2002. An atomistic-based finite deformation membrane for single layer crystalline films. J. Mech. Phys. Solids 50 (9), 1941–1977.
Ashcroft, N.W., Mermin, N.D., 1976. Solid State Physics. Cengage Learning, Brooks/Cole.
Bangert, U., Gass, M.H., Bleloch, A.L., Nair, R.R., Geim, A.K., 2009. Manifestation of ripples in free-standing graphene in lattice images obtained in an aberration-corrected scanning transmission electron microscope. Phys. Status Solidi A 206 (6), 1117–1122.
Bao, W., Miao, F., Chen, Z., Zhang, H., Jang, W., Dames, C., Lau, C.N., 2009. Controlled ripple texturing of suspended graphene and ultrathin graphite membranes. Nat. Nanotechnol. 4 (9), 562–566.
Bowick, M.J., Travesset, A., 2001. The statistical mechanics of membranes. Phys. Rep. 344 (4), 255–308.
Brenner, D.W., Shenderova, O.A., Harrison, J.A., Stuart, S.J., Ni, B., Sinnott, S.B., 2002. A second-generation reactive empirical bond order (REBO) potential energy expression for hydrocarbons. J. Phys.: Condens. Matter 14 (4), 783–802.
Bunch, J.S., Verbridge, S.S., Alden, J.S., van der Zande, A.M., Parpia, J.M., Craighead, H.G., McEuen, P.L., 2008. Impermeable atomic membranes from graphene sheets. Nano Lett. 8, 2458–2462.
Chen, S., Chrzan, D., 2011. Monte carlo simulation of temperature-dependent elastic properties of graphene. Phys. Rev. B 84 (19), 195409.
Fasolino, A., Los, J., Katsnelson, M., 2007. Intrinsic ripples in graphene. Nat. Mater. 6 (11), 858–861.
Freund, L.B., 2013. Entropic pressure between biomembranes in a periodic stack due to thermal fluctuations. Proc. Natl. Acad. Sci. 110, 2047–2051.
Gompper, G., Kroll, D., 1992. Edge correlations of fluid and tethered membranes. J. Phys. I (France) 2 (5), 663–676.
Helfrich, W., 1973. Elastic properties of lipid bilayers: theory and possible experiments. Z. Naturforsch. C 28 (11), 693–703.
Helfrich, W., Servuss, R.M., 1984. Undulations, steric interaction and cohesion of fluid membranes. Il Nuovo Cimento D 3, 137–151.
Humphrey, W., Dalke, A., Schulten, K., 1996. VMD – Visual Molecular Dynamics. J. Mol. Graphics 14, 33–38.
Jiang, J., Wang, J., Li, B., 2009. Thermal expansion in single-walled carbon nanotubes and graphene: nonequilibrium green's function approach. Phys. Rev. B 80 (20), 205429.
Kammler, D.W., 2007. A First Course in Fourier Analysis. Cambridge University Press, New York.
Kirilenko, D.A., Dideykin, A.T., Van Tendeloo, G., 2011. Measuring the corrugation amplitude of suspended and supported graphene. Phys. Rev. B 84 (23), 235417.
Koskinen, P., Kit, O.O., 2010. Approximate modeling of spherical membranes. Phys. Rev. B 82 (23), 235420.
Kownacki, J.-P., Mouhanna, D., 2009. Crumpling transition and flat phase of polymerized phantom membranes. Phys. Rev. E 79, 040101 (R).
Kudin, K.N., Scuseria, G.E., Yakobson, B.I., 2001. C_2F, BN, and C nanoshell elasticity from ab initio computations. Phys. Rev. B 64, 235406.
Le Doussal, P., Radzihovsky, L., 1992. Self-consistent theory of polymerized membranes. Phys. Rev. Lett. 69 (8), 1209–1212.
Lee, C., Wei, X., Kysar, J.W., Hone, J., 2008. Measurement of the elastic properties and intrinsic strength of monolayer graphene. Science 321 (5887), 385–388.
Lipowsky, R., Girardet, M., 1990. Shape fluctuations of polymerized or solidlike membranes. Phy. Rev. Lett. 65 (23), 2893–2896.
Lomholt, M.A., Loubet, B., Ipsen, J.H., 2011. Elastic moderation of intrinsically applied tension in lipid membranes. Phys. Rev. E 83, 011913.
Los, J.H., Katsnelson, M.I., Yazyev, O.V., Zakharchenko, K.V., Fasolino, A., 2009. Scaling properties of flexible membranes from atomistic simulations: application to graphene. Phys. Rev. B 80 (12), 121405.
Lu, Q., Arroyo, M., Huang, R., 2009. Elastic bending modulus of monolayer graphene. J. Phys. D: Appl. Phys. 42 (10), 102002.

Lu, Q., Gao, W., Huang, R., 2011. Atomistic simulation and continuum modeling of graphene nanoribbons under uniaxial tension. Model. Simul. Mater. Sci. Eng. 19 (5), 054006.
Lu, Q., Huang, R., 2009. Nonlinear mechanics of single-atomic-layer graphene sheets. Int. J. Appl. Mech. 1, 443–467.
Lu, Z., Dunn, M.L., 2010. van der Waals adhesion of graphene membranes. J. Appl. Phys. 107 (4), 044301.
Marko, J.F., Siggia, E.D., 1995. Stretching DNA. Macromolecules 28 (26), 8759–8770.
Meyer, J., Geim, A., Katsnelson, M., Novoselov, K., Booth, T., Roth, S., 2007. The structure of suspended graphene sheets. Nature 446 (7131), 60–63.
Mounet, N., Marzari, N., 2005. First-principles determination of the structural, vibrational and thermodynamic properties of diamond, graphite, and derivatives. Phys. Rev. B 71 (20), 205214.
Nelson, D.R., Peliti, L., 1987. Fluctuations in membranes with crystalline and hexatic order. J. Phys. 48 (7), 1085–1092.
Nelson, D.R., Piran, T., Weinberg, S., 2004. Statistical Mechanics of Membranes and Surfaces, 2nd ed. World Scientific Publishing Co., Singapore.
Pathria, R.K., 1996. Statistical Mechanics, 2nd ed. Butterworth-Heineman, Oxford.
Plimpton, S., 1995. Fast parallel algorithms for short-range molecular dynamics. J. Comput. Phys. 117 (1), 1–19.
Pozzo, M., Alfè, D., Lacovig, P., Hofmann, P., Lizzit, S., Baraldi, A., 2011. Thermal expansion of supported and freestanding graphene: lattice constant versus interatomic distance. Phys. Rev. Lett. 106 (13), 135501.
Safran, S.A., 1994. Statistical Thermodynamics of Surfaces, Interfaces, and Membranes. Addison-Wesley Pub., Reading, MA.
Singh, V., Sengupta, S., Solanki, H.S., Dhall, R., Allain, A., Dhara, S., Pant, P., Deshmukh, M.M., 2010. Probing thermal expansion of graphene and modal dispersion at low-temperature using graphene nanoelectromechanical systems resonators. Nanotechnology 21 (16), 165204.
Su, T., Purohit, P.K., 2012. Semiflexible filament networks viewed as fluctuating beam-frames. Soft Matter 8, 4664–4674.
Thompson-Flagg, R.C., Moura, M.J., Marder, M., 2009. Rippling of graphene. Europhys. Lett. 85 (4), 46002.
Timoshenko, S., Woinowsky-Krieger, S., 1987. Theory of Plates and Shells, 2nd ed. McGraw-Hill, New York.
Treloar, L.R.G., 1958. The Physics of Rubber Elasticity. Oxford University Press, New York.
Tuckerman, M., Berne, B.J., Martyna, G.J., 1992. Reversible multiple time scale molecular dynamics. J. Chem. Phys. 97, 1990–2001.
Wei, X., Fragneaud, B., Marianetti, C., Kysar, J., 2009. Nonlinear elastic behavior of graphene: ab initio calculations to continuum description. Phys. Rev. B 80 (20), 205407.
Wei, Y., Wang, B., Wu, J., Yang, R., Dunn, M.L., 2012. Bending rigidity and Gaussian bending stiffness of single-layered graphene. Nano Lett. 13 (1), 26–30.
Weiner, J.H., 2002. Statistical Mechanics of Elasticity. Dover Publications, Mineola, New York.
Zakharchenko, K.V, Katsnelson, M., Fasolino, A., 2009. Finite temperature lattice properties of graphene beyond the quasiharmonic approximation. Phys. Rev. Lett. 102 (4), 046808.
Zakharchenko, K.V., Roldán, R., Fasolino, A., Katsnelson, M.I., 2010. Self-consistent screening approximation for flexible membranes: application to graphene. Phys. Rev. B 82 (12), 125435.
Zan, R., Muryn, C., Bangert, U., Mattocks, P., Wincott, P., Vaughan, D., Li, X., Colombo, L., Ruoff, R.S., Hamilton, B., Novoselov, K.S., 2012. Scanning tunnelling microscopy of suspended graphene. Nanoscale 4 (10), 3065–3068.
Zhao, H., Aluru, N., 2010. Temperature and strain-rate dependent fracture strength of graphene. J. Appl. Phys. 108 (6), 064321.